Volume 16, Number 5, 2023. pp. 539-550

Jordan Journal of Physics

ARTICLE

Fe–Mo/Kaolin Catalyst Optimization and Characterization for the Production of Carbon Nanotube Using the Wet Impregnated Method

Muhammad Bakeko M.[a], **K. U. Isah**[b], **A.S. Abdulkareem**[b], **S. O. Ibrahim**[b], **and Moses E. Emetere**[c,d],

[a] *Department of Physics, The Federal Polytechnic, Bida-Nigerstate, Nigeria.*
[b] *Department of Physics Federal University of Technology, Minna, Nigeria.*
[c] *Department of Physics Bowen University Iwo, Nigeria*
[d] *Department of Mechanical Engineering Science, University of Johannesburg, South Africa.*

Doi: https://doi.org/10.47011/16.5.5
Received on: 05/01/2022; *Accepted on: 08/05/2022*

Abstract: The synthesis of the bimetallic Fe–Mo/kaolin catalyst for carbon nanotube (CNT) production involves the pre-calcination and calcination processes, employing the wet impregnated method. In the pre-calcination stage, we explored the effects of synthesis parameters such as oven drying temperature, mass of kaolin, and heating time using a 2^3 factorial experimental design, ultimately obtaining the highest yield sample. In the calcination phase, the effect of temperature and heating time using a 2^2 factorial experimental design was examined. The as-prepared nanoparticles were characterized by scanning electron microscopy/energy dispersive x-ray spectroscopy (SEM/EDS), thermogravimetric analysis (TGA), differential thermal analysis (DTA), x-ray diffraction (XRD), and Brunauer-Emmet-Teller (BET). SEM/TGA revealed a well-dispersed metallic particle on the kaolin support and its ability to maintain high thermal stability. XRD analysis of the catalyst confirmed its crystal nature and the presence of mixed oxides of different intensities, conducive to CNT growth. The optimum yield obtained after oven drying was 75.25%. At the optimum calcination temperature of 300° C and calcination time of 16 hours, BET analysis determined the surface area and pore volume. For kaolin, the surface area and pore volume were 1.932×10^2 m^2/g and 1.762×10^{-1} cc/g, respectively. The optimal calcine sample showed increment for both the surface area (3.103×10^2 m^2/g) and the pore volume (2.459×10^{-1} cc/g) making it more suitable for CNT production. Lastly, statistical analysis showed that heating time, calcination time, temperature, and mass of kaolin have a significant influence on the catalyst yield in CNT.

Keywords: *catalyst, wet impregnation, optimization, carbon nanotubes*

1. Introduction

The demand for metal nanoparticles is closely tied to their potential applications in catalysis, magnetism, electronics, and other fields [1]. This is attributed to their large surface area and stability. The metal nanoparticle has been synthesized, using various chemical or physical techniques. However, the chemical method is more popular and this is due to its high-yield output. According to [2] the chemical synthesis approach has many advantages such as easier controllability, the capability of scaling up [3], lower reaction temperature, simplicity, cost-effectiveness, etc. This makes it very attractive on the commercial scale. Therefore, significant attention is given to the catalyst in the chemical synthesis of CNT as it serves as a crucial starting

Corresponding Author: Moses Emetere **Email**: mdanasabe@yahoo.com

point for regulating the nanomaterial's structure and morphology [4]. The output yield is determined by the elemental composition and the optimization of control parameters, making the synthesis of nanoparticles with specific characteristics a primary focus [5]. As a catalyst, the metal nanoparticle used in the production of carbon nanotubes (CNT) is made up of transition metal elements, which could either come from a single element or in the form of a combination of elements, supported on different inert materials. Various types of catalysts employed in the synthesis of CNTs can be categorized based on their composition. Catalysts may consist of single metallic transitional metal elements, such as Fe, Co, Mo, and Ni. Additionally, combinations of two or more metallic elements are used as catalysts, including two-metallic combinations like Fe-Co, Ni-Fe, Co-Mo, Fe-Mo, and Co-Ni, three-metallic combinations (e.g., Fe-Co-Ni, Co-Mo-Fe), or even four-metal mixtures (e.g., Fe-Co-Ni-Mo). These metal nanoparticles, contribute [6] to the growth of CNTs in a way that the presence of more than one metal species can significantly improve the activity of the prepared catalyst so that the particles obtained are in dispersed form. Metal nanoparticles [7] are typically presented together with different support materials, such as zeolites, MgO, Al_2O_3, SiO_2, $Al(OH)_3$, $CaCO_3$, CaO, and others [8]. These support materials act as platforms or substrates for the growth of the CNTs when using the CVD method. Choosing the right catalyst and support material is crucial for producing high-quality CNTs with optimal yield. The selection is based on properties such as inertness, high surface area, stability under reaction and regeneration conditions, and low synthesis cost. To reduce the cost associated with carbon nanotube (CNT) synthesis, especially for large-scale production, we utilize kaolin. Kaolin is known for its high composition of silicon oxide and alumina [9], making it an excellent substrate due to the strong metal support interaction, along with high surface area and good metal dispersion. In one study the variation of synthesis parameters for Fe-Co bimetallic catalyst on $CaCO_3$ prepared through a wet impregnation method, was investigated using 2^4 factorial design of experiment [10]. The optimal conditions for catalyst preparation were found to be a drying time of 12 hours, calcination temperature of 100°C, stirring speed of 1000 rpm, and a mass of CaCO3 support of 10 g, resulting in a maximum catalyst yield of 99.6%. The same study revealed that among the investigated parameters, the stirring speed and mass of the support had the most significant impact on the catalyst yield.

Metal nanoparticles that are used as catalysts for CNT synthesis are assessed based on their interaction in carbide formation and carbon solubility. While other factors such as temperature, diffusion, and particle size variations are also deemed important, metal elements capable of forming carbides are recognized as efficient catalysts [11]. Fe is a member of the group where a relatively large fraction of carbon dissolves into the metal cluster to form carbide, while Mo belongs to the group where carbide formation occurs rapidly at low carbon concentration.

Some studies identified the viability of bimetallic catalysts involved in the production of CNT [12, 13]. Other researchers (see Refs. [2, 9]) used a 2^4 experimental design in an investigation of the effect of parameter variation over a bimetallic fe-Co/Kaolin catalyst by catalytic chemical vapor deposition (CCVD) [14]. Their results confirmed a high catalyst yield and the formation of well-dispersed mixed oxides, which favor CNT production.

This article presents a factorial design of experiments for synthesizing a catalyst for CNTs via CVD using a Fe-Mo/kaolin catalyst. This represents the initial step in CNT synthesis to establish an optimum sample for producing MWCNT with the best yield. To the best of our knowledge, there have been no investigations carried out so far regarding Fe-Mo/kaolin as a catalyst material for the synthesis of CNT. In this paper, the first section is a general introduction dealing with different combinations of precursor elements for the synthesis of catalysts in CNT materials production. The second section is about the materials used and the preparation methods to achieve the optimum sample. Section three is the discussion of results from various characterizations. Finally, we provide an outlook on the synthesis of the new catalyst material.

2. Materials and methods

2.1 Materials

The materials used in this study include:

- Ferric nitrate nanohydrate: $Fe(NO_3)_3 \cdot 9H_2O$
- Hexaammonium heptamolybdate tetrahydrate: $(NH_4)_6Mo_7O_{24} \cdot 4H_2O$
- Kaolin of analytical grade with a percentage purity in the range of 98 to 99.0%

All chemicals were utilized without additional purification, and a Drier Box AX-ov73 was employed in the experimental procedures.

2.2 Preparation of Catalyst

The wet impregnated method by [10, 15] was used with little modification for the preparation of the catalyst to grow the CNT. In this method, equal proportions by weight of Fe and molybdenum were prepared by dissolving 6.1793g of $(NH_4)_6Mo_7O_{24}.4H_2O$ and 2.02 g of $Fe(NO_3)_3.\ 9H_2O$ in 50 mL distilled water. 8 g of kaolin was immediately added to the solution, and the mixture was left for 30 min to age under constant stirring in a magnetic stirrer. The resulting gel was dried inside an oven at 100°C for 10 h, then it was left to cool to room temperature. It was then ground and sieved through a 150 µm. The catalyst was then calcined at 300°C for 16 h. Thereafter it was left to cool to room temperature and kept for characterisation.

2.3 Preparing of Optimized Sample

Minitab 17 design software was used for the 2^3 factorial experimental design shown in Table 1 to generate experimental runs, where the effects of the synthesis parameters on the yield of the catalyst were investigated, namely mass of support, temperature, and time. A combined 8.19 g of bimetallic Fe-Mo salt in 50 ml volume of distilled water was mixed with 8-12 g mass of the kaolin support in variation to form the prepared eight (8) different samples of the bimetallic Fe-Mo/kaolin catalyst. The catalyst was continuously mixed for 30 min under a magnetic stirrer until it formed a slurry, and then the samples were heated at 120°C for 12 h to obtain the oven-dry catalyst samples. The percentage yield of all the samples was calculated using the relationship presented in Eq. (1).

$$\text{Yield \%}_{\text{oven drying}} = \frac{M_{before} - M_{after}}{M_{before}} \text{ x } 100 \qquad (1)$$

TABLE 1. 2^3 factorial experiment design with variations of mass of support, temperature, heating time, and percentage yield after oven drying.

Run order	Mass(gram)	Time (hour)	Temperature oC	$\%yield_{oven\ drying}$
1	8	8	100	72.24
2	12	8	100	67.38
3	8	10	100	75.25
4	12	10	100	72.17
5	8	8	120	72.46
6	12	8	120	67.66
7	8	10	120	71.60
8	12	10	120	67.74

where M_{after} is the mass of catalyst after oven drying and M_{before} is the mass of catalyst before oven drying.

Minitab17-design software was used for the calcination stage to determine a suitable sample that has the highest yield after oven drying as presented in Table 2. In this stage, we varied the calcination temperature and heating time to determine the sample with the better pore area and pore volume after calcination to produce a better CNT yield.

TABLE 2. 2^2 factorial experimental design table with variation in temperature and heating time

Run order	Time(hour)	Temperature °C
1	12	300
2	12	500
3	16	300
4	16	500

2.4 Characterisation of the Optimized Fe-Mo/Kaolin Catalyst and Kaolin

The catalyst was obtained with a support mass of 8 g, an oven drying time of 10 h, and an oven drying temperature of 100°C, resulting in the sample with the highest yield which is considered the optimized sample. Subsequently, the optimized sample was calcined at varying temperatures of 300°C and 500°C for 12 h and 16 h. The characterizations revealed its outstanding properties, leading to the selection of the best sample after calcination for the synthesis of the catalyst used in the production of MW-CNT. All samples were characterized as follows: A sample of kaolin, the highest yield catalyst sample after oven drying (Co), and calcined samples designated as C1 (calcined at 300°C/12h), C2 (calcined at 500°C/12h), C3 (calcined at 300°C/16h), and C4 (calcined at 500°C/16h). To assess the thermal stability of the sample, thermal gravimetric analysis (TGA) was conducted using a TGA 4000 instrument from Perkin Elmer, USA. The surface area was determined through Brunauer-Emmett-Teller (BET) analysis using a NOVA 4200e instrument from Quantachrome Instruments, USA. The degree of crystallinity and morphology were examined using an x-ray diffractometer (XRD; PW 1800 diffractometer, Philips, Netherlands) and a scanning electron microscope coupled with an electron diffraction spectrometer (SEM/EDS; JEM 100S, JEOL Ltd., Japan), respectively.

3. Results and Discussions

3.1 The Effect of Mass of Support

Table 1 presents variations in the sample catalyst, including support mass (8-12 g), oven drying time from (8-10 h), oven drying temperature (100-120°C), and the corresponding yield percentage of oven dry samples. The yield percentage for the entire sample with 8 g support mass consistently exceeded 70%. In contrast, all samples with a support mass of 12 g yielded below 70%, except for the catalyst at 10 h and 100°C, which exhibited a value of 72.17%. This suggests that the catalyst yield with 8 g of support mass is higher compared to the sample catalyst with 12 g support mass (bimetallic catalyst Fe-Mo) at constant drying time and temperature.

The conclusion drawn from the results is that an increase in support mass from 8 g to 12 g while keeping other variables constant does not support the physical separation of nanoparticles. This observation indicates particle agglomeration into larger crystallites, resulting in a reduced number of surface metal atoms per unit mass of metal. Consequently, this leads to a decrease in the number of active sites on the catalyst and a lower catalyst yield.

3.2 Effect of Oven Drying Time

Table 1 also displays the influence of oven drying time on the catalyst yield, with the following results. The variations in catalyst yield are presented in groups of two oven drying times, specifically 8 hours and 10 hours. Although the table does not explicitly display the catalyst yield for oven drying time, subtracting the first two experiments reveals a 4.86% reduction in yield for the 8-hour time period. Furthermore, the last three rows in Table 2 show subsequent variation factors of 3.08%, 4.80%, and 3.86%, respectively.

Notably, the highest yield is observed at 10 hours, with a value of 75.25%. This suggests a notable rate of dispersion of active metals onto the substrate support, as evidenced by SEM showcasing a fully mixed composite and XRD revealing the presence of new compounds. Additionally, it indicates that the rate at which water is removed from the pores during the 10-hour pre-calcination time was faster, resulting in an increased concentration of precursors until saturation. This, in turn, led to an elevated catalyst yield.

3.3 The Effect of Pre-calcination Temperature

In addition to the influence of catalyst support and the influence of the oven drying time, the impact of the oven drying temperature on the catalyst yield is also presented in Table 1. The data indicated that, for all samples, the oven drying temperature is either 100°C or 120°C across all experiments. The results indicate that temperatures of 100°C and 120°C are sufficient for the optimum catalyst yield of 75.25% and 72.46%, respectively. These results suggest that the interactions between the catalyst support and active metals are enhanced at both 100°C and 120°C, leading to higher catalyst yields. The likely explanation is that the increase in temperature is sufficient to overcome binding energy barriers, thereby accelerating the rate of evaporation during the synthesis process.

3.4 The Effect of Calcination Temperature and Time

Table 2 displays results pertaining to the influence of calcination temperature on catalyst yield. The table indicates that, for all samples, the calcination temperature ranges between 300°C and 500°C, with a duration of either 12 h or 16 h for all experiments. The results indicate that the rate of water elimination from the pores of nanoparticles during the 12-hour to 16-hour calcination process contributes to an increased surface area ($3.103\ x10^{2}$) and pore volume ($2.459\ x10^{-1}$) of precursors. These changes in surface area and pore volume, as evidenced by BET analysis, are indicative of optimal catalyst conditions for CNT production.

3.5 Brunauer-Emmet-Teller (BET) Analysis of Kaolin and Optimized Fe-Mo/Kaolin Catalyst

Table 3 presents the BET analysis results, displaying the surface area and pore volume of kaolin and Fe-Mo catalyst with kaolin support carried out under the N_2 atmosphere. For kaolin, the initial surface area and pore volume are $1.932x10^{2}$ m^2/g and 1.762×10^{-1} cc/g, respectively. There is a significant increase in these values for the as-prepared sample (C_o) to 2.573×10^{2} m^2/g and 2.123×10^{-1} cc/g. Subsequently, there is a decrease in sample C1 (calcined at 300°C/12 h) to 2.481×10^{2} m^2/g and 2.189×10^{-1} cc/g, followed by a further reduction in sample C_2 (calcined at 500°C/12 h) to 2.342×10^{2} m^2/g and 1.979×10^{-1} cc/g. However, sample C_3 (calcined at 300°C/16 h) shows a significant increase in surface area (3.103×10^{2} m^2/g) and pore volume (2.459×10^{-1} cc/g). There is then a reduction in sample C_4 (calcined at 500°C/16 h) with a surface area of 2.35×10^{2} m^2/g and a pore volume of 2.180×10^{-1} cc/g. Overall, all samples exhibit a significant increase in surface area and pore volume compared to kaolin, with sample C_3 demonstrating the most favorable characteristics for carbon nanotube (CNT) production. This enhancement may be attributed to the creation of micropores and mesopores, particularly favored by high temperatures.

TABLE 3. BET result for Fe-Mo catalyst with kaolin support.

Sample/ catalyst	Surface area (m^2/g)	Pore volume (cc/g)
Kaolin	$1.932x10^{2}$	$1.762x10^{-1}$
Co	$2.573x10^{2}$	$2.123x10^{-1}$
C1	$2.481x10^{2}$	$2.189x10^{-1}$
C2	$2.342x10^{2}$	$1.979x10^{-1}$
C3	$3.103x10^{2}$	$2.459x10^{-1}$
C4	$2.35x10^{2}$	$2.180x10^{-1}$

3.6 Thermogravimetric Analysis (TGA) and Differential Thermal Analysis (DTA) of Optimum Fe-Mo/Kaolin Catalyst

Thermogravimetric analysis (TGA) is a technique that reveals sample transformations in response to changes in applied heat. The TGA diagram typically shows a continuous decrease in the sample's weight as the temperature rises. Concurrently, the data from indicate changes in the sample relative to its weight, manifesting as either heat absorption (endothermic reaction) or heat release (exothermic reaction). The TGA characterization profile of kaolin (the support material) used for the bimetallic catalyst was obtained over a temperature range of 0 to 900ºC at a constant heating rate of 10 mL min^{-1} under N_2 flow and is depicted in Fig. 1.

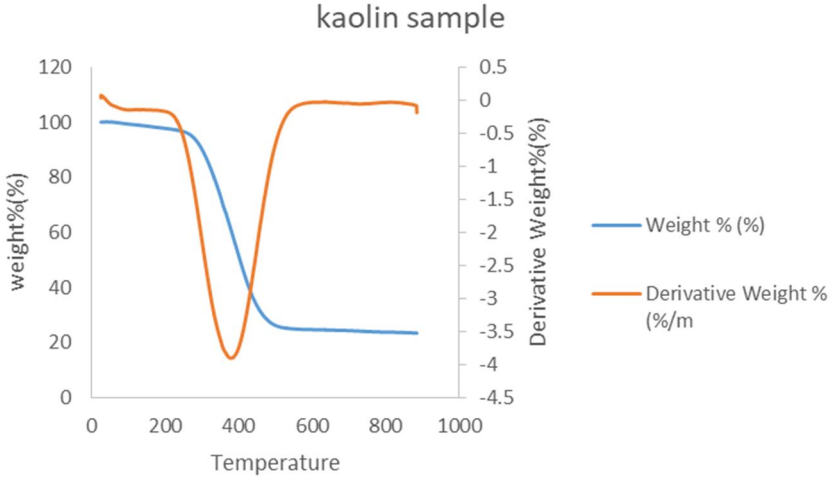

FIG. 1. TGA/DTA for kaolin.

Fig. 1 displays the TGA/DTA graph of the support material (kaolin). The graph reveals that kaolin remains stable from 25.5°C to 237.97ºC with minimal loss. Beyond this point, as the temperature rises further (from 237.97°C to 470.91°C), kaolin begins to decompose. During this decomposition phase, a weight loss of 69.122% is recorded, attributed to the removal of absorbed water molecules and volatile organic matter embedded in the kaolin. The weight loss may also be linked to the formation of compounds such as $Fe_2(MoO_4)_3$ and MoO_3 through the oxidative decomposition of the iron and molybdenum nitrates mixture, with the elimination of O_2 and NO_2. Beyond 481.27°C, no further significant weight loss is observed, indicating that kaolin becomes thermally stable at this temperature. This observation influenced the selection of 300ºC for the development of the Fe-Mo/kaolin catalyst, which is intended for use in CNT production.

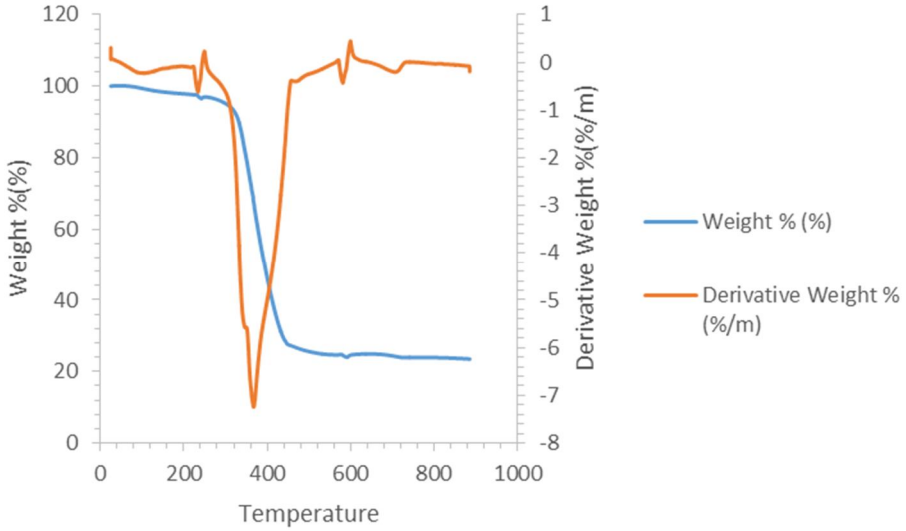

FIG. 2. TGA/ DTA for sample C_3.

Fig. 2 represents the TGA/DTA of the sample calcined at a temperature of 300°C for 16 h. The diagram indicates that sample C_3 remains stable from 25.5°C to 305.15ºC without a significant loss. As the temperature continues to rise (310.53°C-446.19°C), decomposition initiates. Further increases in temperature do not result in additional weight loss. The observed 76% weight loss during this period is likely attributed to the elimination of absorbed water molecules and volatile organic matter within the kaolin. Additionally, the weight loss may be associated with the formation of compounds such as $Fe_2(MoO_4)_3$ and MoO_3, resulting from the oxidative decomposition of the iron and molybdenum nitrates mixture with the elimination of O_2 and NO_2. The DTA data complement this, revealing a significant exotherm at a temperature of 366.58°C.

3.7 X-ray Diffraction (XRD) Analysis for Fe-Mo/Kaolin Catalyst

The structure and crystal-phase composition of the metal nanoparticle supported on kaolin were determined through XRD analysis. Fig. 3(a) shows representative data for the as-prepared sample and the sample calcined at 300°C for 16 h. All diffraction peak intensities were detected at 2θ. The XRD spectra for the optimized sample show characteristic peaks at 2θ values of 9.4593°, 12.6836°, 19.1667°, 23.1458°, 25.6155, and 27.1934°. The 2θ values at 19.1667° and 49.2839° represent the characteristic peaks of the crystalline bimetallic catalyst $Fe_2(MoO_4)_3$. Additionally, the 2θ values at 12.6836°, 23.1458°, 25.6155°, 27.1934°, 29.0114°, and 33.5396° correspond to the compound MoO_3. The orderly distribution of the bimetallic catalyst on the pores of the support indicates the crystalline nature of the prepared catalyst. The highest peak occurs on the (1 2 2) plane. The d-spacing was calculated for each peak as presented in Table 4 using Bragg's law in Eq. (2).

$$\lambda = 2dsin(\theta) \quad (2)$$

where λ represents the wavelength of the x-ray beam, d is the distance between the adjacent atomic interlayer, and θ represents the diffraction angle. Table 4 reveals that, as the scanning angle increases, the distance between planes of atoms responsible for diffraction peaks

decreases. The Rietveld refinement, as illustrated in Fig. 3(b), was performed to further analyze crystal chemical changes. Notably, changes were observed on the (4 2 0) plane, where the d-spacing values were determined to be 4.488 and 2.132, respectively.

The phase changes for different calcination conditions are presented in Fig. 3(c), where the phase change is subdivided into regions A, B, C, D, E, F, G, H, and I. In region A, it is observed that calcination at 500°C for 16 hours leads to the re-crystallization of the Fe-atom, suggesting a more pronounced Fe-O bond at this stage. The corresponding phase changes observed in regions A-I provide strong evidence that the microstructural features of the polycrystalline compound are coherently producing diffracting domain sizes under specific calcination conditions. This observation suggests that the compound exhibits a significant distribution of microstrain, which may be advantageous for applications such as solar cells.

TABLE 4. D-spacing of peaks.

Plane	D(A)	Plane	D(A)
(0 1 1)	9.075	(7 1 6)	2.568
(1 0 1)	8.335	(2 2 14)	2.427
(0 3 3)	5.850	(3 0 5)	2.331
(0 2 6)	5.167	(4 2 0)	2.132
(2 0 1)	4.594	(1 2 7)	2.086
(4 2 0)	4.488	(1 5 3)	1.853
(2 1 1)	4.139	(2 4 4)	1.696
(4 4 2)	3.482	(7 10 5)	1.603
(1 2 3)	3.119	(0 1 11)	1.595
(1 2 11)	3.087	(5 9 14)	1.556
(1 1 12)	2.948	(4 12 8)	1.497
(2 7 1)	2.749	(3 3 4)	1.449
(3 7 2)	2.608	(2 5 7)	1.369

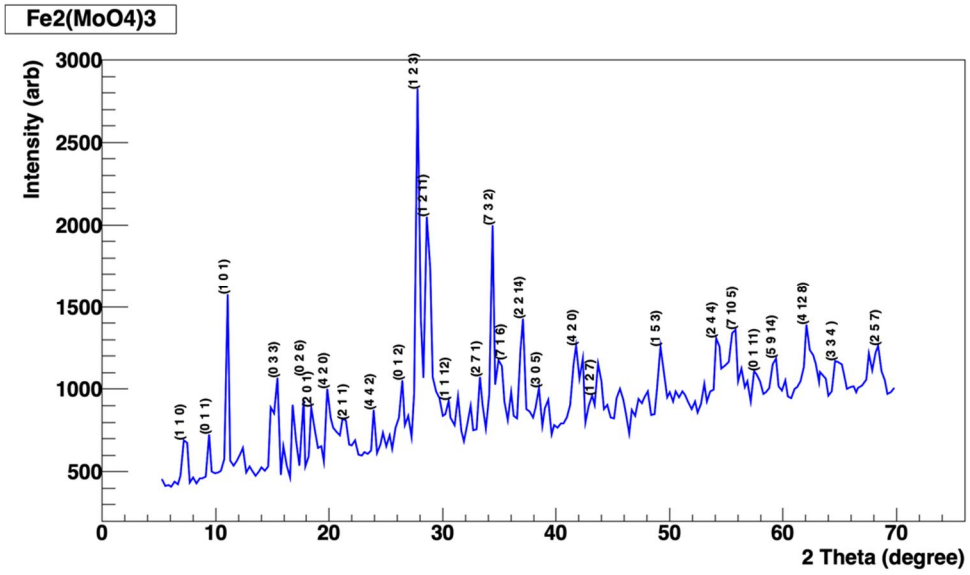

FIG. 3(a). XRD pattern for sample C_o.

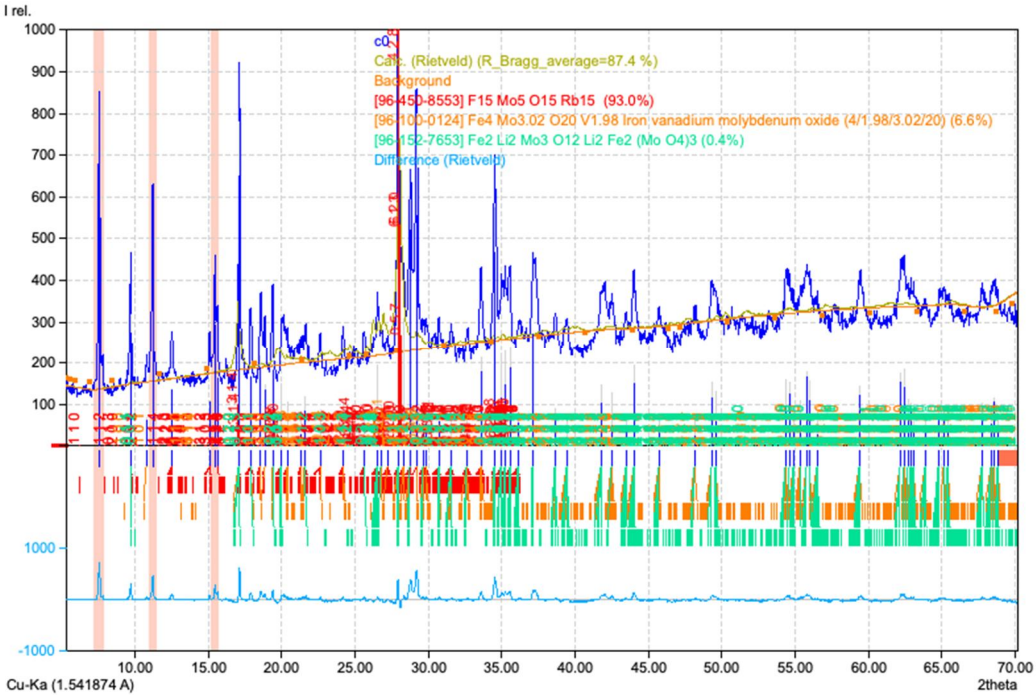

FIG. 3(b). Rietveld refinement of planar pattern for the as-prepared sample.

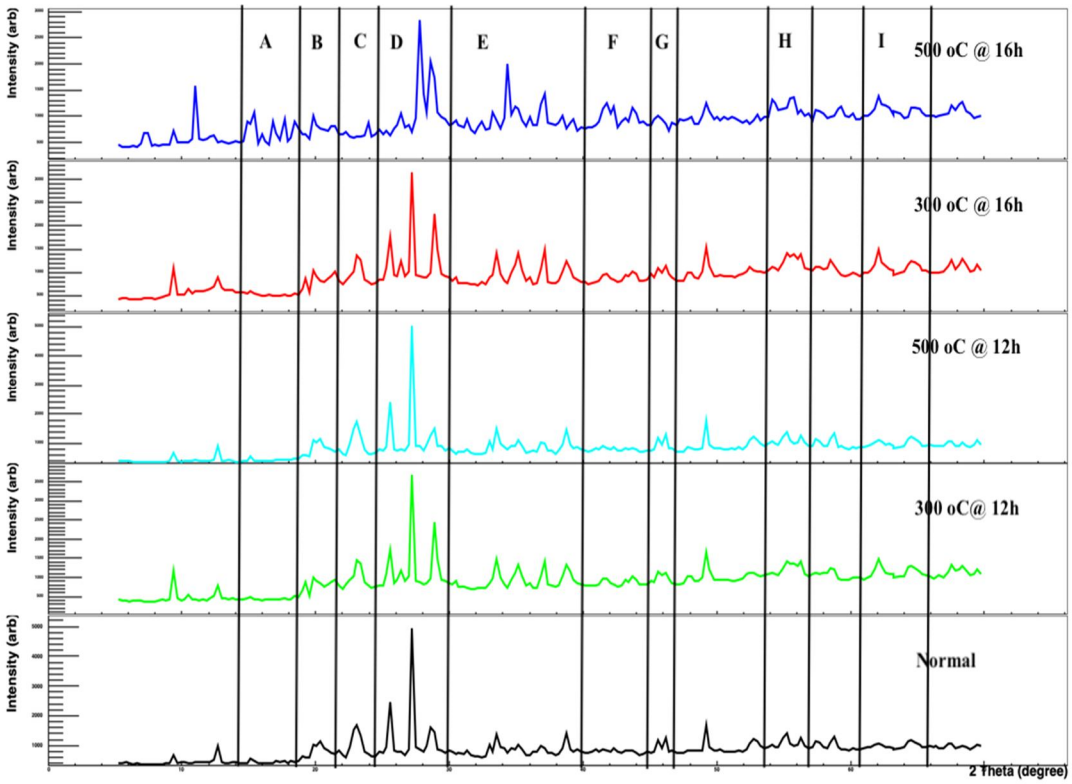

FIG. 3(c). XRD pattern for as-prepared sample.

The microstrain distribution observed may be attributed to the interactions of Mo with different metals and oxides, leading to the formation of new compounds such as MoO_4 or $Fe_2(MoO_4)_3$ [16]. Additionally, the unidentified peaks shown in Fig. 3(a) may be indicative of the influence of kaolin in the compound. The SEM analysis of the catalyst and metal precursors reveals a homogeneous mixture [17] in nanoflakes, showcasing enhanced pores within the support. This results in metal particles with an increased surface area and pore volume.

3.8 Scanning Electron Microscopy (SEM) Image Analysis for Fe-Mo/Kaolin Catalyst

Unlike optical microscopy, where the focus is on photons of light, SEM utilizes an energetic electron beam focused on the sample specimen, leading to different effects. One of these effects involves emitted secondary electrons generated when a primary electron changes its path, releasing part of its energy to an atom in the specimen as heat. Each incident electron can produce several secondary electrons, making them abundant and the most commonly used imaging signal in SEM. Another effect is the generation of backscattered electrons, which occurs as a result of the collision between an incident electron and an atom in the specimen. In this process, the electron loses part of its energy and is scattered backward at a 180-degree angle. Some of the backscattered electrons can generate additional secondary electrons upon exiting the specimen [18]. On the specimen, regions with higher atomic numbers of chemical elements will appear brighter in the SEM images.

The SEM images provide a morphological view of both the as-prepared catalyst (Co) and the optimum calcined catalyst C_3 [Fig. 4(a)]. The image displays good miscibility of the kaolin, Fe, and Mo phases. At the same time, the magnified micrographs reveal the presence of scattered and uniformly oriented nanoflakes in the Fe-Mo/kaolin composite, showing well-distributed nanoflakes grown on the substrate (kaolin). The micrographs further reveal that, within the nanoflakes formed, the metal catalysts are uniformly distributed on the surface of the kaolin. The random distribution of the nanoflakes indicates a highly porous surface material, meeting the essential requirement for a catalyst used in CNT synthesis.

The particulate size distribution is presented in Fig. 4(b), revealing seven groups of particulates whose orientation is influenced by the individual atomic sizes of each element. A total of 385 particulates were observed in the analysis.

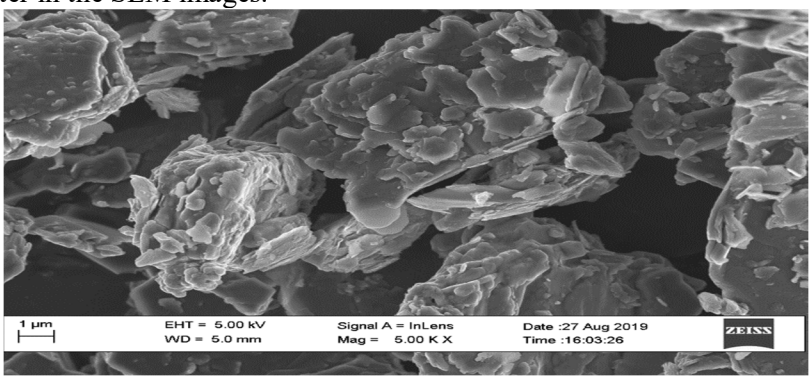

FIG. 4(a). SEM image of sample Co.

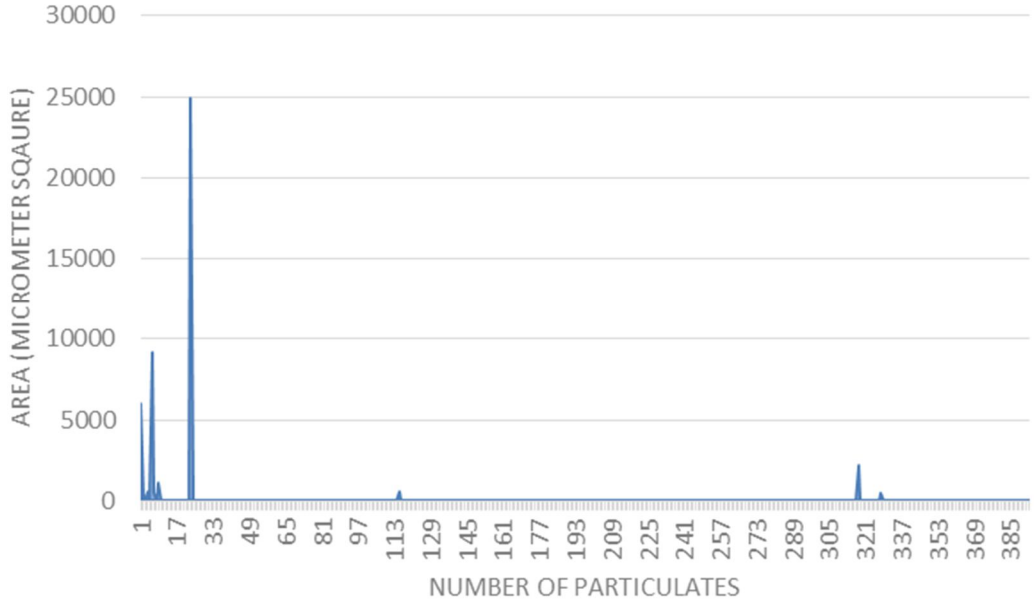

FIG. 4(b). Number of particulates per size distribution.

Fig. 5(a) shows the SEM image of the compounds that underwent calcination at 300°C for 12 hours. The observation indicates that the calcination process has transformed sections of the compound from a heterogeneous to a homogeneous state. Concurrently, the particulate sizes have disintegrated into smaller sizes, as presented in Fig. 5(b). This outcome aligns with the XRD results, suggesting the presence of a microstrain distribution that may be advantageous for the device.

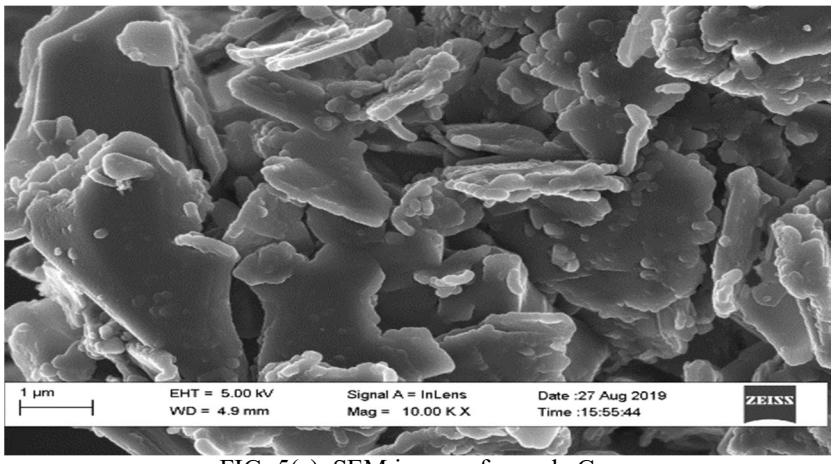

FIG. 5(a). SEM image of sample C_3.

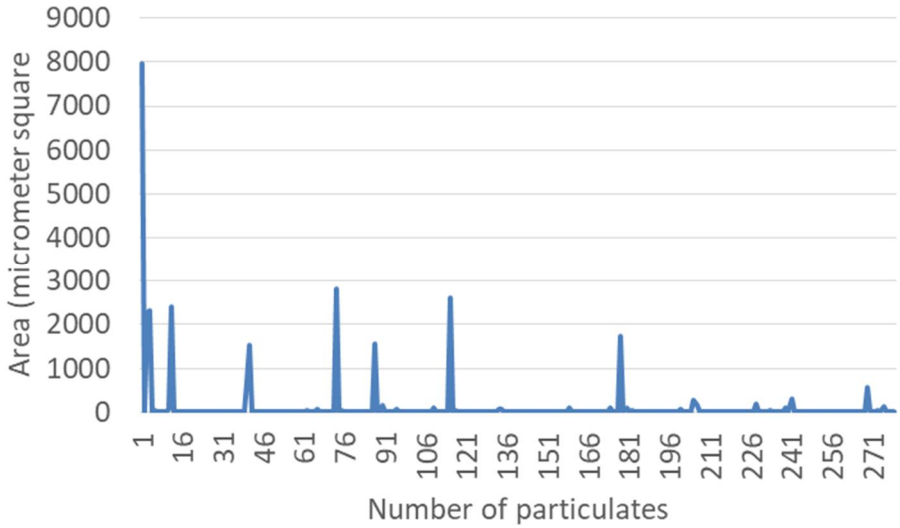

FIG. 5(b). Number of particulates per size distribution.

3.9 Energy Dispersive X-Ray Spectroscopy (EDS) Spectrum for Fe-Mo/Kaolin Catalyst

When an incident electron beam is directed towards an atom in a solid, electron transitions occur with the release of x-rays. For example, if an incident electron knocks out an electron from the K-shell (n = 1 shell) of a metal atom, a vacancy or hole is created in that shell. When another electron from a higher shell fills in that vacancy (electron transitions), X-rays are emitted. These transitions are named K X-rays for transitions to the K-shell (n = 1), L X-rays for transitions to the L-shell (n = 2), and M X-rays for transitions to the M-shell (n = 3). These transitions form the characteristic x-rays of each chemical element and are the main reason for the development of energy-dispersive x-ray (EDX) spectroscopy detection systems in electron microscopy, expanding its use in materials microstructural characterization [18]. EDS is used to determine the quantity of each elemental particle in the prepared catalyst using energy-dispersive x-ray (EDX) spectroscopy. The results typically show the presence of different elemental compositions and their percentage compositions. In the diagram, the prepared catalyst particles consist of different elements, such as Fe, Mo, Ti, Si, Al, O, K, and C in varying proportions. The elements K, Ti, Al, and Si possibly originated from the support material kaolin, while Fe and Mo are obtained from their

respective salts. The element C in the EDS spectra may have come from the carbon coating procedure employed during sample preparation. Furthermore, the high weight percentage of oxygen in the catalysts may be due to the formation of oxides of the catalyst (Fe_2O_3 and Mo_3O_4) during calcination. Additionally, the oxygen could have come from the support material kaolin (which contains oxides of Al_2O_3 and SiO_2). The absence of nitrogen in the sample confirms the effective removal of most nitrates in Fe and Mo salts during the calcination process. This result also indicates that the particles contain both Fe and Mo at a 1:8 ratio, sufficient to produce some quantity of CNT. The addition of molybdenum helps improve the growth of carbon nanotubes [16], with the reported average synthesized atomic ratios of Mo to Fe being close to 1:1.

The presence of heavy metals in the EDX spectra, particularly around the lower energy position along with oxygen, suggests that oxygen is in a mixed oxide form of the elements C, Fe, Al, Si, and Mo. This indicates the presence of ternary compounds $Fe_2(MoO_4)_3$ and MoO_4, which are oxides of Fe and Mo [12]. However, Fe (6.4 keV and 7.1 keV), Mo (17.5 keV and 19.6 keV), and K (3.3 keV) are also observed in the spectra.

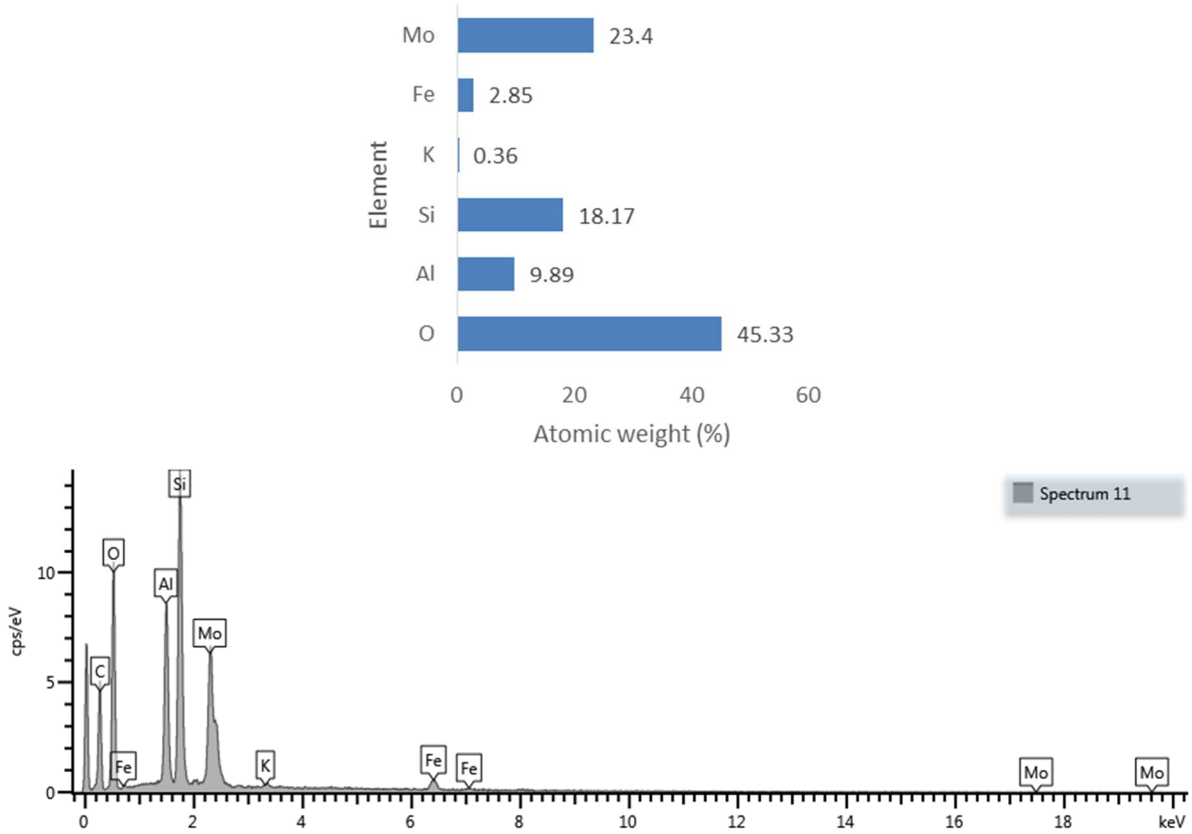

FIG. 6. EDX Graph with atomic weight (%) showing each element for the sample calcined at 300°C/16h.

4. Conclusion

In conclusion, this report underscores the reliability of the 2^3 factorial experimental design for parametric optimization of solar cell fabrication processes. Through strict adherence to the control parameters such as the oven drying temperature, heating time, and mass of support, it is reported that the optimum catalyst yield reached 75.5%. This optimal catalyst yield is expected to correspond to a surface area and pore volume of metallic particles (Fe–Mo) at 3.103 $x10^2$ m^2/g and 2.459 $x10^{-1}$cc/g, respectively. Microstructural analysis reveals the presence of seven groups of particulates, each oriented according to the individual atomic sizes of the elements involved. The metallic particles (Fe–Mo) demonstrate elemental stability within the temperature range of 25.5°C to 305.15°C, exhibiting minimal loss. The characterization techniques used showed that the compound forms an excellent composition for growing CNTs due to the combination of encapsulated metal alloys within this framework. These

discoveries are therefore germane in the furtherance of research on CNTs. The report concludes by recommending the exploration of different synthetic routes in future work.

Acknowledgement

This paper is sponsored by PTDF GRANT PTDF/SP&D/AOGRG/V.VI/117

References

[1] Li, Y., Liu, J., Wang, Y., Wang, Z.L. and Drive, F., Chem. Mater., 13 (3) (2001) 1008.

[2] Srdić, V., Boskovic, G., Bajac, B., Kónya, Z., Panic, S., Rakić, S. and Kukovecz, Á., React. Kinet. Mech. Cat. 122 (2) (2017) 775.

[3] Brhane, Y. and Gabriel, T., Int. Res. J. Pharm., 7 (7) (2016) 19.

[4] Teo, K.B.K., Chhowalla, M. and Milne, W.I., Encyclopedia of Nanoscience and Nanotechnology, X (2003) 1.

[5] Paper, C., Burakova, E.A. and Tugolukov, E.N., AIP Conf. Proc., 1899 (2017) 020008.

[6] Varshney, K., Int. J. Eng. Res., 2 (4) (2014) 660.

[7] Eatemadi, A., Daraee, H., Karimkhanloo, H., Kouhi, M., Zarghami, N., Akbarzadeh, A., Abasi, M., Hanifehpour, Y. and Joo, S.W., Nanoscale Res. Lett., 9 (1) (2014) 393.

[8] Toussi, S.M., FakhruL-Razi, A., Luqman, C.A. and Suraya, A.R., Sains Malaysiana, 40 (3) (2011) 197.

[9] Oyewemi, A., Abdulkareem, A.S., Tijani, J.O., Bankole, M.T., Abubakre, O.K., Afolabi, A.S. and Roos, W.D., Arab. J. Sci. Eng., 44 (2019) 5411.

[10] Bankole, M.T., Mohammed, I.A., Abdulkareem, A.S., Tijani, J.O., Ochigbo, S.S., Abubakre, O.K. and Afolabi, A.S., J. Alloy. Compd., 749 (2018) 85.

[11] Curtarolo, S., Awasthi, N., Setyawan, W., Jiang, A., Bolton, K., Tokune, T. and Harutyunyan, A.R., Phys. Rev. B, 78 (2008) 054105.

[12] Obasogie, O.E., Abdulkareem, A.S., Mohammed, I.A., Bankole, M.T., Jimoh, O. and Abubakre, O.K., Carbon Lett., 28 (2018) 72.

[13] Bernardo, G.P.O. and Abella, L.C., IJCEA, 3 (6) (2012) 446.

[14] Chen, J., Xu, X., Zhang, L. and Huang, S., Nano-Micro Lett., 7 (4) (2015) 353.

[15] Ibrahim, S.O., Abdulkareem, A.S., Isah, K.U., Ahmadu, U., Bankole, M.T. and Kariim, I., Adv. Nat. Sci: Nanosci. Nanotechnol., 9 (2018) 025008.

[16] Thomas Koilraj, T. and Kalaichelvan, K., IEEE Intern. Conf. Advances in Engineering, Science and Management (ICAESM -2012), (2012) 429.

[17] Kathyayini, H., Reddy, K.V., Nagy, J.B. and Nagaraju, N., Indian J. Chem., 47A (2008) 663.

[18] Girão, A.V., Caputo, G. and Ferro, M.C., Compr. Anal. Chem., 75 (2017) 153.